We are IntechOpen, the world's leading publisher of Open Access books Built by scientists, for scientists

6,900
Open access books available

185,000
International authors and editors

200M
Downloads

Our authors are among the

154
Countries delivered to

TOP 1%
most cited scientists

12.2%
Contributors from top 500 universities



WEB OF SCIENCE™

Selection of our books indexed in the Book Citation Index in Web of Science™ Core Collection (BKCI)

Interested in publishing with us?
Contact book.department@intechopen.com

Numbers displayed above are based on latest data collected.
For more information visit www.intechopen.com



Chapter 2

Adaptive Robust Guidance Scheme Based on the Sliding Mode Control in an Aircraft Pursuit-Evasion Problem

Jian Chen, Yongjun Zheng, Yuan Ren, Yuan Tian, Chen Bai, Zhang Ren, Guangqi Wang, Nannan Du and Yu Tan

Additional information is available at the end of the chapter

http://dx.doi.org/10.5772/intechopen.72177

Abstract

In this chapter, a robust guidance scheme utilizing a line-of-sight (LOS) observation is presented. Initial relative speed and distance, and error boundaries of them are estimated in accordance with the interceptor-target relative motion kinematics. A robust guidance scheme based on the sliding mode control (SMC) is developed, which requires the boundaries of the target maneuver, and inevitably has jitter phenomenon. For solving above-mentioned problems, an estimation to the target acceleration's boundary is developed for enhancing robustness of the guidance scheme and the Lyapunov stabilization is analyzed. The proposed robust guidance scheme's brief characteristic is to reduce the effect of relative speed and distance, to reduce the effect of target maneuverability on the guidance precision, and to strengthen the influence of line-of-sight angular velocity. The proposed scheme's performances are validated by the simulations of different target maneuvers under two worst-case conditions.

Keywords: robust guidance scheme, line-of-sight angular velocity, sliding mode control, boundary of target maneuver, Lyapunov stability

1. Introduction

The traditional Proportional Navigation Guidance (PNG) schemes including their extensions have been widely employed in interceptors because of their efficiencies and simplifications (only need line-of-sight information). PNG makes the normal load of interceptor proportional to the line-of-sight (LOS) angular velocity [1]. Nevertheless, the target can add the miss distance by acting evading maneuver because the target maneuvers are ahead of the guidance commands from PNG. For achieving desired interception performances, even for

INTECH
open science | open minds

© 2018 The Author(s). Licensee InTech. This chapter is distributed under the terms of the Creative Commons Attribution License (http://creativecommons.org/licenses/by/3.0), which permits unrestricted use, distribution, and reproduction in any medium, provided the original work is properly cited. CC BY

the target maneuver, it is necessary to develop advanced guidance schemes [1, 2]. These advanced guidance schemes usually require more information, like relative speed and distance, target's acceleration, or time-to-go.

For passive seekers, which are equipped with electro-optical or infrared sensors, the line-of-sight **a**ngular velocity can be observed only. If an estimation equation is assumed to estimate target kinematics, relative speed and distance and target's acceleration will be identified. The commonly used estimation model is a Kalman filter. At the same time, one must select a target's motion model, like the current statistical model, the Singer model, or the interactive multi-model scheme [3]. For polishing up the estimating performance of the target's maneuvers, observability of the interception problem with LOS angular velocity measurement is analyzed [4]. It concludes that current homing guidance schemes result in a decrease in observability of tracking the target. Because relative distance cannot be observed from the line-of-sight measurement, it is necessary to use a special type of self-motion to solve this problem. Thus, the method of introducing LOS angular oscillatory motion is presented in [4] to improve the observability. The oscillatory motion of the LOS angle improves observability, but the trajectories generated by the guidance schemes are inevitably influenced by this motion mode and affect final guidance precision. Therefore, the target maneuver estimation is constrained by a lot of practical limitations.

The sliding mode control (SMC) is robust to disturbances. Therefore, it is employed to develop adaptive guidance schemes for target's unpredictable maneuver without requirements to estimate the target's acceleration. Recently, many guidance schemes based on the SMC have been proposed, for instance, the guidance schemes based on the adaptive and optimal SMC [5–7], the high-order SMC [8, 9], SMC-based integrated guidance and control (IGC) [10, 11], and SMC with impacting angle constraint [12–14].

SMC-based optimal and adaptive guidance schemes have become a focus since the 1990s. An adaptive sliding mode guidance (ASMG) scheme is presented in [5] for target maneuvering and parameter disturbance of the guidance system. In addition, an optimal sliding mode guidance (OSMG) scheme is deduced from the ASMG, and the optimal guidance coefficients are given in [6]. In [7], the Fuzzy OSMG (FOSMG) formulated by the OSMG and PNG is stated by adjusting the weights of the OSMG and PNG using fuzzy logic. It is noted that the FOSMG owns the advantages of the PNG for nonmaneuvering targets and the OSMG for maneuvering targets. The ASMG, OSMG, and FOSMG have practical advantages of simple expressions. Nevertheless, it is essential to identify the target's normal load to adjust weights of the FOSMG.

The higher order sliding mode guidance (HOSMG) scheme is a current research highlight. While the SMC-based first-order guidance is a balance between smoothing jitter and ensuring robustness through switching frequently, the HOSMG generates control commands smoothly to systems with relative degree arbitrarily. A smooth guidance scheme based on a second-order sliding mode is developed for solving the uncertainties of the actuator and the target's maneuver [8]. In [9], a terminal guidance law with known convergent time is proposed by using the finite-time mean-square practical convergence as sliding surfaces. It validates that HOSMG is robust to stochastic noises and bounded uncertainty and does not have high-frequency jitters. The HOSMG's flaw exists in converging slowly for real time due to complex algorithms.

Integrated guidance and control (IGC) which is based on the SMC has become an unusual approach for developing a guidance system. The traditional timescale separation method splits the guidance system into an inner loop autopilot and an outer loop command system. The IGC system merges the two loops into a unique loop. Based on self-motion and relative motion states, the IGC produces commands to aero surfaces straight. Zero effort miss is used to be a sliding surface for developing the IGC [10, 11]. Due to the complex coupling between guidance and control states, this method does not spread more widely than an intuitive timescale separation method.

Based on the SMC, the guidance scheme with impacting angle constraint is designed to solve the problem of directional impacting. In practical cases, a specific impacting angle is desired to directionally hit the target or to better detect thee target. Under the impacting angle constraint, the result from ideal initial attack conditions can meet the interception requirements for nonmaneuvering and step-maneuvering targets [12–14]. However, the guidance accuracy of the target's complicated maneuver will decrease.

To sum up, although guidance schemes based on the SMC and target's maneuver estimation algorithms act excellently in simulation, the computation degrees of them have become too complex to realize. In fact, one needs a simple-expression guidance scheme based on the SMC, and if not requiring the target acceleration, it will be better. In addition, the discontinuous characteristic induced by the sliding mode part can cause jitter of guidance commands that is detrimental to the aero fins. The coefficient of sliding mode part indicates target acceleration's boundary. Actually, it is hard to get the boundary. If setting the boundary too great, the autopilot might be saturated; if setting the boundary too tiny, the sliding mode's presence cannot be guaranteed. With the target acceleration's unknown boundary, for ensuring the stability, the simplified guidance schemes based on the SMC including the FOSMG, OSMG, and ASMG have greater sliding mode part, which might cause jitter. Adaptive control offers a solution. The unknown parameters can be estimated in the online identification for the uncertain system. Nevertheless, it has no capability to suppress disturbances. Thus, the adaptive control to identify the upper boundary of the system uncertainty is merged with the SMC to suppress disturbances [15].

An interceptor-target pursuit-evasion game which only employs the line-of-sight angular velocity is under consideration in this chapter. The target maneuver is treated as a bounded perturbation. More states are demanded, including initial relative speed and distance and error boundaries of them. It is derived from recursive estimation of relative motion kinematics and obtains approximations of relative speed and distance. A simplified sliding mode guidance scheme is given, which requires target acceleration's boundary and inevitably has jitter phenomenon. For overcoming the above shortcomings, an adaptive parameter is utilized to estimate target acceleration's boundary and to adaptively adjust in terms of the line-of-sight angular velocity; moreover, the Lyapunov stabilization has been analyzed. The proposed guidance scheme's brief characteristic is to decrease the effect of relative speed and distance on the guidance precision and to strengthen the influence of line-of-sight angular velocity.

This chapter's rest part is listed hereafter. The problem statement is given in Section 2. Two robust guidance schemes based on the SMC are presented in Section 3. Section 4 carries out simulations, and conclusions are given in Section 5.

2. Pursuit-evasion game

2.1. Relative motion kinematics

The interceptor's movement consists of two orthogonal channels. The pursuit-evasion game is decomposed into two 2D channels.

Figure 1 shows the geometric diagram of the interceptor-target relative motion kinematics. A Cartesian reference system is denoted by "*X-O-Y.*" The interceptor and target are denoted by "*M*" and "*T*". The line-of-sight angle is denoted by "q". The relative distance is denoted by "r". Flight path angles of the interceptor and target are denoted by "φ_m" and "φ_t". Velocities of the interceptor and target are denoted by "V_m" and "V_t".

Endgame relative motion kinematics are given by

$$\begin{cases} \dot{r} = V_t \cos\left(\varphi_t - q\right) - V_m \cos\left(\varphi_m - q\right), \\ r\dot{q} = V_t \sin\left(\varphi_t - q\right) - V_m \sin\left(\varphi_m - q\right). \end{cases} \tag{1}$$

Let the relative speed $v = \dot{r}$. Eq. (2) is obtained as

$$\begin{cases} \dot{v} = r\dot{q}^2 + \left[\dot{V}_t \cos\left(\varphi_t - q\right) - V_t\dot{\varphi}_t \sin\left(\varphi_t - q\right)\right] \\ \quad - \left[\dot{V}_m \cos\left(\varphi_m - q\right) - V_m\dot{\varphi}_m \sin\left(\varphi_m - q\right)\right], \\ r\ddot{q} = -2\dot{r}\dot{q} + \left[\dot{V}_t \sin\left(\varphi_t - q\right) + V_t\dot{\varphi}_t \cos\left(\varphi_t - q\right)\right] \\ \quad - \left[\dot{V}_m \sin\left(\varphi_m - q\right) + V_m\dot{\varphi}_m \cos\left(\varphi_m - q\right)\right]. \end{cases} \tag{2}$$

For simplification, we get

$$\dot{v} = r\dot{q}^2 + a_{tr} - a_{mr}, \tag{3}$$

$$\ddot{q} = -2\frac{v}{r}\dot{q} + \frac{1}{r}a_{tq} - \frac{1}{r}a_{mq}, \tag{4}$$

where acceleration components of the interceptor and target along the line-of-sight are denoted by "a_{mr}" and "a_{tr}"; acceleration components of the interceptor and target orthogonal to the line-of-sight are denoted by "a_{mq}"and "a_{tq}". The equations of them are formulated as

$$a_{tr} = \dot{V}_t \cos\left(\varphi_t - q\right) - V_t\dot{\varphi}_t \sin\left(\varphi_t - q\right), \tag{5}$$

$$a_{mr} = \dot{V}_m \cos\left(\varphi_m - q\right) - V_m\dot{\varphi}_m \sin\left(\varphi_m - q\right), \tag{6}$$

$$a_{tq} = \dot{V}_t \sin\left(\varphi_t - q\right) + V_t\dot{\varphi}_t \cos\left(\varphi_t - q\right), \tag{7}$$

$$a_{mq} = \dot{V}_m \sin\left(\varphi_m - q\right) + V_m\dot{\varphi}_m \cos\left(\varphi_m - q\right). \tag{8}$$

Assume the line-of-sight angular velocity is accurately observed at each instant. Initial relative speed and distance and error boundaries of them are obtained as

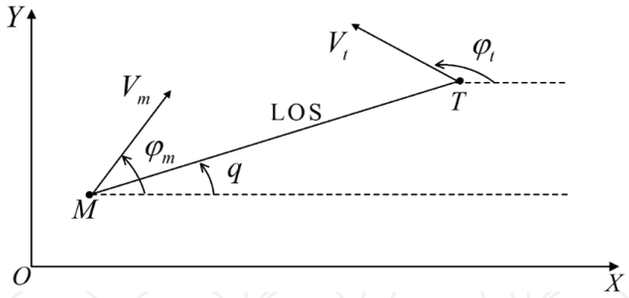


Figure 1. Relative motion kinematics.

$$\begin{cases} r_0 = \overline{r}_0 + \tilde{r}_0, & |\tilde{r}_0| \le \delta_{r_0}, \\ v_0 = \overline{v}_0 + \tilde{v}_0, & |\tilde{v}_0| \le \delta_{v_0}, \end{cases} \tag{9}$$

where initial relative speed and distance are denoted by "v_0" and "r_0"; observations of v_0 and r_0 are denoted by "$\overline{v}_0$" and "$\overline{r}_0$"; observation deviations of v_0 and r_0 are denoted by "$\tilde{v}_0$" and "$\tilde{r}_0$"; upper boundaries of $\tilde{v}_0$ and $\tilde{r}_0$ are denoted by "δ_{v_0}" and "δ_{r_0}".

Remark 1. $\overline{v}_0$ and $\overline{r}_0$ are detected by a radar on ground or aircraft carrier and are sent to the interceptor via the data link only once. δ_{v_0} and δ_{r_0} are treated to be maximum observation deviation of the detector.

2.2. Kinematics simplification

For successfully intercepting the target, the line-of-sight angular velocity should be constrained [5, 6]. In this chapter, seeker and autopilot loops are not considered. With this premise, relative equation of the line-of-sight angular velocity $\dot{q}$ is obtained as Eq. (4). However, $1/r$ and $2v/r$ in Eq. (4) are obtained as Eq. (3), which indicates relative speed v alters as r, v, $\dot{q}$, a_{tr}, and a_{mr} vary, and v_0 and r_0 are preset. In accordance with the characteristic of an interceptor's engine, the thrust along the line of sight almost does not change. Moreover, the target is usually escaping orthogonally to the line of sight to increase the line-of-sight angular velocity. Although acceleration component of the target along the line-of-sight is subsistent, the relative speed does not change too much with limited energy and time. Assume that acceleration components along the line of sight of the target and interceptor are zero. Simplify Eq. (3) into

$$\begin{cases} \dot{r} = v, \\ \dot{v} = r\dot{q}^2. \end{cases} \tag{10}$$

Define $z_1 = r$ and $z_2 = v$. Equation (10) becomes

$$\begin{cases} \dot{z}_1 = z_2, \\ \dot{z}_2 = z_1\dot{q}^2. \end{cases} \tag{11}$$

According to Eq. (9), initial states for Eq. (11) to get $\overline{r}_0$ and $\overline{v}_0$ are obtained as

$$z_1^{(1)}(t_0) = \overline{r}_0,\ z_2^{(1)}(t_0) = \overline{v}_0, \tag{12}$$

$$z_1^{(2)}(t_0) = \overline{r}_0 + \delta_{r0},\ z_2^{(2)}(t_0) = \overline{v}_0 + \delta_{v0}, \tag{13}$$

$$z_1^{(3)}(t_0) = \overline{r}_0 - \delta_{r0},\ z_2^{(3)}(t_0) = \overline{v}_0 - \delta_{v0}. \tag{14}$$

Equations (12)–(14) are employed to calculate Eq. (11). Boundaries of v and $r$are computed as

$$\begin{cases} |\Delta r| = \max\left\{z_1^{(2)} - z_1^{(1)}, z_1^{(1)} - z_1^{(3)}\right\}, \\ |\Delta v| = \max\left\{z_2^{(2)} - z_2^{(1)}, z_2^{(1)} - z_2^{(3)}\right\}. \end{cases} \tag{15}$$

3. Guidance scheme design

3.1. Guidance scheme based on the sliding mode control

A sliding surface is determined by

$$s = z_1^{(1)}\dot{q}. \tag{16}$$

In accordance with Eq. (16), forcing s to zero represents that $\dot{q}$ or $\overline{r}$ prompts to 0. In terms of quasi-parallel approach guideline, the line-of-sight angular velocity will be adjusted to 0 to guarantee that the interceptor hits the target [5, 6].

Theorem 1. A sliding mode control-based guidance (SMCG) scheme described by

$$a_{mq} = \left[\left(N - \frac{z_1^{(2)}}{z_1^{(3)}}\right)\left|z_2^{(1)}\right| + 2|\Delta v|\right]\dot{q} + \varepsilon sgn(\dot{q}), \tag{17}$$

where $z_2^{(1)}$, $z_1^{(2)}$, and $z_1^{(3)}$ are deduced from Eq. (11) with Eqs. (12–14), $N > 2$ is an integer, $|\Delta v|$ is obtained from Eq. (15), and ε is a_{tq}'s upper boundary, guarantees that $s = z_1^{(1)}\dot{q}$ is driven to 0.

Proof. Compute Eq. (11) with Eq. (9) and define $\overline{v} = z_2^{(1)}$ and $\overline{r} = z_1^{(1)}$.v and r are obtained as

$$r = \overline{r} + \tilde{r}, v = \overline{v} + \tilde{v}, \tag{18}$$

where derivations between estimations and real values are denoted by "$\tilde{v}$" and "$\tilde{r}$".

In terms of the deduction in Section 2, we have

$$|\tilde{r}| \le |\Delta r|, |\tilde{v}| \le |\Delta v|. \tag{19}$$

Define a Lyapunov function:

$$V_1 = 0.5s^2. \tag{20}$$

Since $\overline{v} < 0$, an approach scheme is defined as

$$\dot{s} = \frac{\overline{r}}{r}\{ - \left(N - 2 + \frac{z_1^{(2)}}{z_1^{(3)}} - \frac{r}{\overline{r}} \right)|\overline{v}|\dot{q} - 2\left(|\Delta v| - \tilde{v}\right)\dot{q} - \left[\varepsilon sgn(\dot{q}) - a_{tq}\right]\}. \tag{21}$$

Then,

$$\dot{V}_1 = -\frac{\overline{r}^2}{r}\left(N - 2 + \frac{z_1^{(2)}}{z_1^{(3)}} - \frac{r}{\overline{r}} \right)|\overline{v}|\dot{q}^2 - 2\frac{\overline{r}^2}{r}\left(|\Delta v| - \tilde{v}\right)\dot{q}^2 - \frac{\overline{r}^2}{r}\left[\varepsilon sgn(\dot{q}) - a_{tq}\right]\dot{q}. \tag{22}$$

Equation (11) is solved with Eq. (12) or (14). Then, we get

$$0 < z_1^{(3)} \le \overline{r}. \tag{23}$$

Equation (11) is solved with Eq. (9) or (13). Because $|\tilde{r}_0| \le \delta_{r0}$, we have

$$z_1^{(2)} \ge r > 0. \tag{24}$$

Next, the following is obtained:

$$\frac{z_1^{(2)}}{z_1^{(3)}} - \frac{r}{\overline{r}} \ge 0. \tag{25}$$

Since $N > 2$, then

$$N - 2 + \frac{z_1^{(2)}}{z_1^{(3)}} - \frac{r}{\overline{r}} > 0. \tag{26}$$

Because $\varepsilon sgn(\dot{q}) - a_{tq} > 0$, $|\Delta v| - \tilde{v} > 0$, $\overline{r} > 0$, and $r > 0$, we get $\dot{V}_1 < 0$. Using Lyapunov stability theory, we can guarantee that $V_1 \to 0$. Finally $s \to 0$. Since $s = z_1^{(1)}\dot{q}$, that is, $\dot{q} \to 0$.

Remark 2. The "sgn" function in Eq. (17) is replaced by the following function to suppress the jitter:

$$a_{mq} = \left[\left(N - \frac{z_1^{(2)}}{z_1^{(3)}} \right)\left| z_2^{(1)} \right| + 2|\Delta v| \right]\dot{q} + \varepsilon \frac{\dot{q}}{|\dot{q}| + \Delta}, \tag{27}$$

where Δ is a tiny positive constant.

3.2. Improved guidance scheme based on the SMCG

ε in Eq. (27) or (17) is unchanged, which indicates that an unchanged upper boundary of a_{tq} is employed to ensure the sliding mode's subsistence. By this means, the guidance command's jitter might exist in the vicinity of the sliding mode although "sgn" is already replaced in Eq. (27). For smoothing the command, the better way is to use the adaptive approach to dynamically estimate ε [23, 24].

Proposition 1. An unchanged constant $k > 0$ exists, so that

$$\left|a_{tq}\right| \le (N-2+k)|\overline{v}||\dot{q}|, \tag{28}$$

where upper boundaries' estimations of a_{tq} are formulated by $(N-2+k)|\overline{v}|\dot{q}$.

Theorem 2. An improved sliding mode control-based guidance (ISMCG) scheme described by

$$\begin{cases} a_{mq} = \left[\left(N - \dfrac{z_1^{(2)}}{z_1^{(3)}} + \widehat{k}\right)\left|z_2^{(1)}\right| + 2|\Delta v|\right]\dot{q}, \\ \dot{\widehat{k}} = \dfrac{1}{\gamma}\dfrac{\overline{r}^2}{r}|\overline{v}|\dot{q}^2, \end{cases} \tag{29}$$

where $z_2^{(1)}$, $z_1^{(2)}$, and $z_1^{(3)}$ are deduced from Eq. (11) with Eqs. (12–14), $N > 2$ is an integer, $|\Delta v|$ is obtained from Eq. (15), and $\gamma > 0$ is a constant, guarantees that $s = z_1^{(1)}\dot{q}$ is driven to 0.

Proof. Define $\tilde{k} = k - \widehat{k}$ and the Lyapunov function:

$$V_2 = 0.5\left(s^2 + \gamma\tilde{k}^2\right). \tag{30}$$

Then,

$$\dot{V}_2 = -\frac{\overline{r}^2}{r}\left(\frac{z_1^{(2)}}{z_1^{(3)}} - \frac{r}{\overline{r}}\right)|\overline{v}|\dot{q}^2 - 2\frac{\overline{r}^2}{r}(|\Delta v| - \tilde{v})\dot{q}^2 - \frac{\overline{r}^2}{r}\left[\left(N - 2 + \widehat{k}\right)|\overline{v}|\dot{q} - a_{tq}\right]\dot{q} + \gamma\tilde{k}\dot{\tilde{k}}. \tag{31}$$

According to Eq. (28) and $\dot{\widehat{k}} = \frac{1}{\gamma}\frac{\overline{r}^2}{r}|\overline{v}|\dot{q}^2$, we get

$$\begin{aligned} \dot{V}_2 &\le -\frac{\overline{r}^2}{r}\left(\frac{z_1^{(2)}}{z_1^{(3)}} - \frac{r}{\overline{r}}\right)|\overline{v}|\dot{q}^2 - 2\frac{\overline{r}^2}{r}(|\Delta v| - \tilde{v})\dot{q}^2 - \frac{\overline{r}^2}{r}\left(\widehat{k} - k\right)|\overline{v}|\dot{q}^2 + \gamma\tilde{k}\dot{\tilde{k}} \\ &= -\frac{\overline{r}^2}{r}\left(\frac{z_1^{(2)}}{z_1^{(3)}} - \frac{r}{\overline{r}}\right)|\overline{v}|\dot{q}^2 - 2\frac{\overline{r}^2}{r}(|\Delta v| - \tilde{v})\dot{q}^2. \end{aligned}$$

In accordance with condition (25), because $|\Delta v| - \tilde{v} > 0$, $\overline{r} > 0$, and $r > 0$, we get $\dot{V}_2 < 0$. Using Lyapunov stability theory, we can guarantee that $V_2 \to 0$. Finally $s \to 0$. Since $s = z_1^{(1)}\dot{q}$, that is, $\dot{q} \to 0$.

Remark 3. $\overline{r}$ is employed to take the place of the real r in Eq. (29).

4. Simulations

4.1. Initial conditions

Simulations will be conducted to validate the feasibility and superiority of the proposed schemes in this part. In simulations, the maximum acceleration limit of the interceptor is 10 g

for verifying the performance of the interceptor with a rather constrained maneuverability. Assume that the target is less agile than the interceptor. Control systems of them are expressed by the following first-order systems:

$$\frac{a_{ma}(s)}{a_{mq}(s)} = \frac{1}{\tau_m s + 1}, \tag{32}$$

$$\frac{a_{ta}(s)}{a_{tq}(s)} = \frac{1}{\tau_t s + 1}, \tag{33}$$

where the guidance commands are denoted by "a_{tq}" and "a_{mq}" and the responses are denoted by "a_{ta}" and "a_{ma}". $\tau_t = 0.5$ and $\tau_m = 0.2$.

Initial conditions are preset to $r_0 = 3000$ m, $v_0 = \dot{r}_0 = -350$ m/s, $q_0 = 10^\circ$, $\dot{q}_0 = -3\text{deg/s}$, $V_t = 500$ m/s, and $\varphi_t = 0^\circ$. In accordance with the Eq. (9), $\delta_{v0} = 70$ m/s and $\delta_{r0} = 300$ m are given as upper boundaries of $|\tilde{v}|$ and $|\tilde{r}|$. In Eqs. (27) and (29), $N = 3$, $\varepsilon = 8$ g, $\Delta = 0.0001$, and $\gamma = 125$. Two worst-case conditions of the initial observed relative speed $\overline{v}_0$ and distance $\overline{r}_0$ are given.

Condition 1 (C1):

$$\overline{r}_0 = r_0 - \delta_{r0}, \overline{v}_0 = v_0 - \delta_{v0}. \tag{34}$$

Condition 2 (C2):

$$\overline{r}_0 = r_0 + \delta_{r0}, \overline{v}_0 = v_0 + \delta_{v0}. \tag{35}$$

Following maneuver modes of the target, including case 1, case 2, and case 3, are used to test the performance of the proposed schemes. Assume that the interceptor is detected by the target in 2 s and then the target begins to escape.

Case 1: Square maneuver in the direction of the axis Y.

$$\begin{cases} a_{ty}(t) = 0, & t \le 2s \\ a_{ty}(t-2) = -a_{ty}(t), a_{ty}(2) = 6\text{g}. & t > 2s \end{cases} \tag{36}$$

Case 2: Sine maneuver in the direction of the axis Y.

$$\begin{cases} a_{ty}(t) = 0, & t \le 2s \\ a_{ty}(t) = 8\text{g} \cdot \sin[3(t-2)]. & t > 2s \end{cases} \tag{37}$$

Case 3: Step maneuver in the direction of the axis Y.

$$\begin{cases} a_{ty}(t) = 0, & t \le 2s \\ a_{ty}(t) = 8\text{g}. & t > 2s \end{cases} \tag{38}$$

4.2. Comparisons between the OSMG and the APNG

Compare the ISMCG and SMCG with the APNG and OSMG. The actual target normal load and relative speed are considered known in the APNG; thereby, neither Condition 1 nor Condition 2 can affect the APNG. For the OSMG, it owns a simplified formulation which has robustness to target's maneuver, and it is popular in practice. Its simplified realization for online is as follows [6].

$$a_{mq} = -3\dot{\overline{r}}_0\dot{q} + \varepsilon sgn(\dot{q}) \simeq -3\overline{v}_0\dot{q} + \varepsilon\frac{\dot{q}}{|\dot{q}| + \Delta}, \tag{39}$$

where the initial observed relative speed is denoted by "$\overline{v}_0$". ε and Δ have no difference with those of the SMCG.

The expression of the APNG is obtained as [16]

$$a_{mq} = N'|v|\dot{q} + N'\frac{a_{tq}}{2}, \tag{40}$$

where the actual target normal load and the relative speed are denoted by "a_{tq}" and "v". An optimal value of the constant N' is 3 [16].

Schemes	Case 1		Case 2		Case 3	
	Condition 1	Condition 2	Condition 1	Condition 2	Condition 1	Condition 2
APNG	0.0831	0.0831	2.7448	2.7448	0.0173	0.0173
OSMG	0.0525	0.0819	0.0129	0.1148	0.0010	0.0015
ISMCG	0.0050	0.0003	0.0010	0.0019	0.0020	0.0036
SMCG	0.0289	0.0645	0.1115	0.1253	0.0010	0.0013

Table 1. Comparisons of miss distances (m).

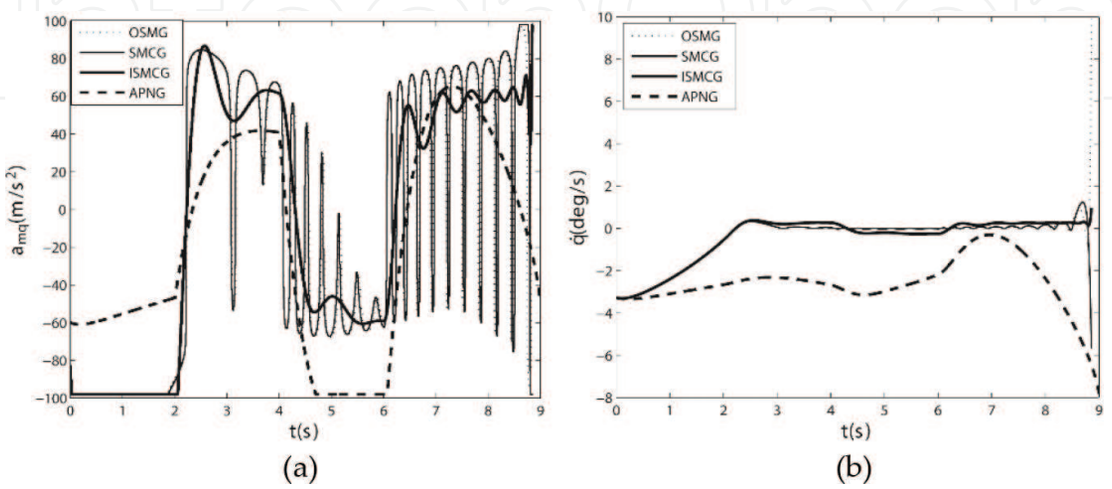


Figure 2. Guidance commands and line-of-sight angular velocities in case 1 under condition 1. (a) Guidance commands (b) Line-of-sight angular velocities.

http://dx.doi.org/10.5772/intechopen.72177

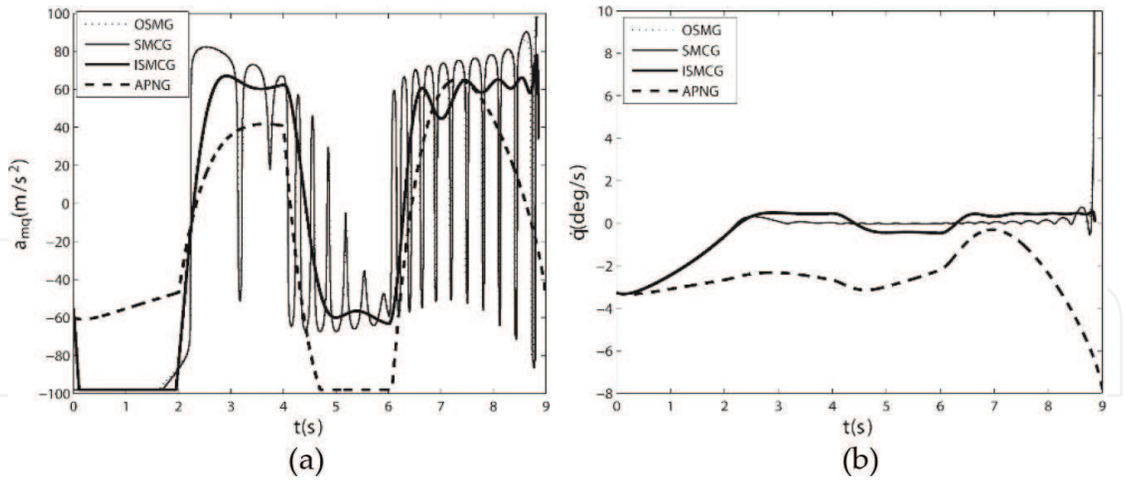


Figure 3. Guidance commands and line-of-sight angular velocities in case 1 under condition 2. (a) Guidance commands (b) Line-of-sight angular velocities.

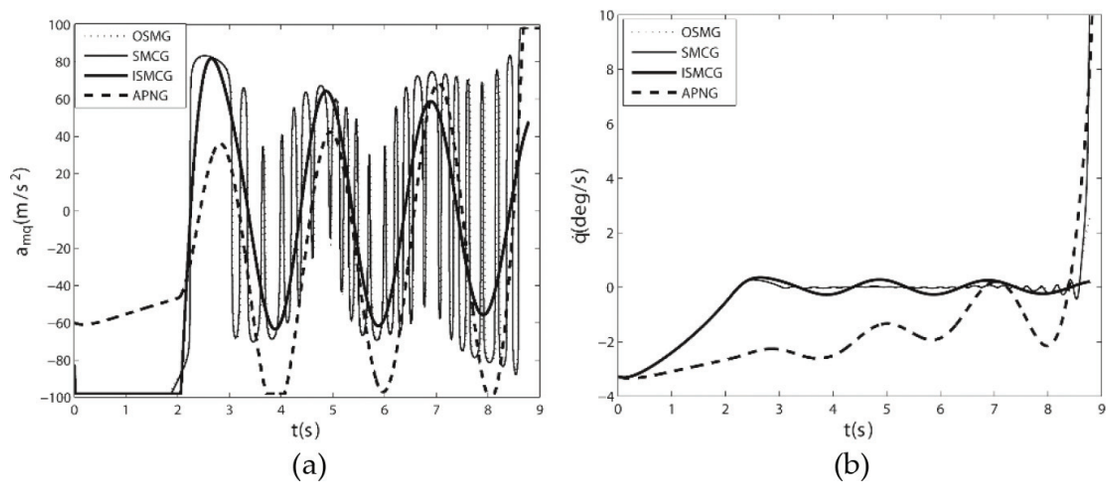


Figure 4. Guidance commands and line-of-sight angular velocities in case 2 under condition 1. (a) Guidance commands (b) Line-of-sight angular velocities.

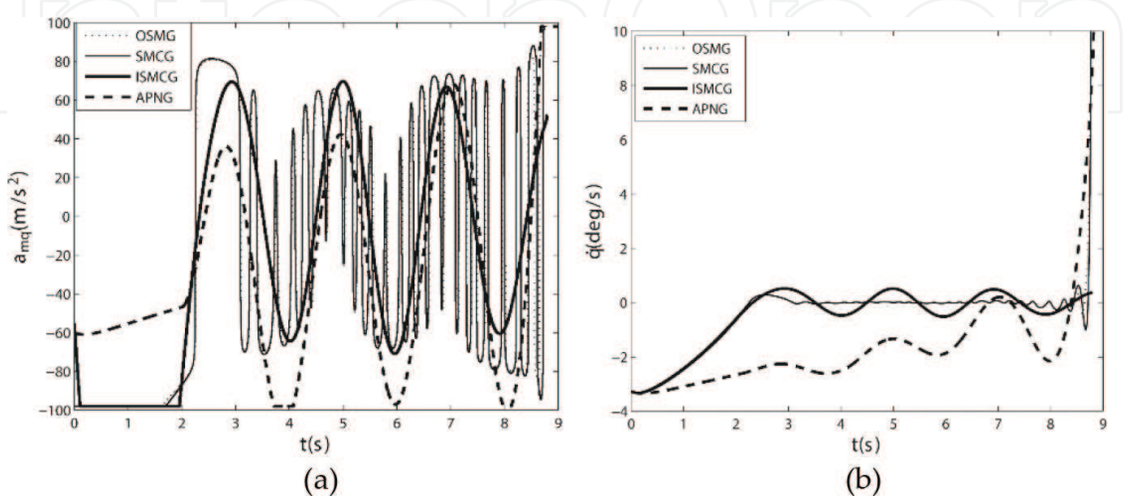


Figure 5. Guidance commands and line-of-sight angular velocities in case 2 under condition 2. (a) Guidance commands (b) Line-of-sight angular velocities.

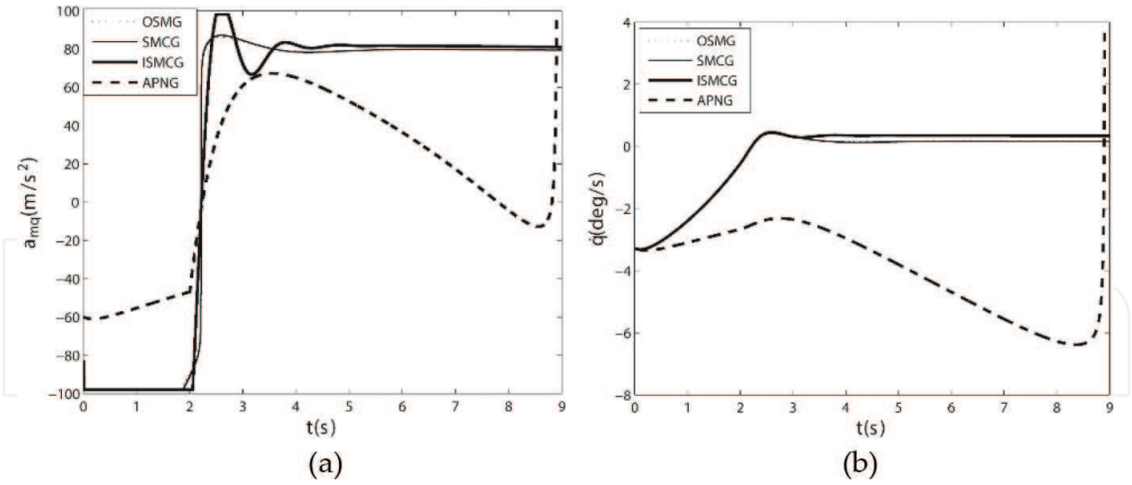


Figure 6. Guidance commands and line-of-sight angular velocities in case 3 under condition 1. (a) Guidance commands (b) Line-of-sight angular velocities.

The missing distance is illustrated in **Table 1**, and the guidance commands and the line-of-sight angular velocities are shown in **Figures 2–7**. As shown in **Table 1**, these four guidance schemes all accomplish the interception task with the constraint $|a_{mq}| \leq 10$ g. In case 2, APNG's miss distances are comparatively greater, because Eq. (40) is deduced assuming a_{tq} is unchanged [17]. Nevertheless, the target might have a complicated maneuvering kind of escape. For the APNG, there is a greater miss distance to case 2, rather than to case 1 and case 3. It indicates the ANPG's limitations on intercepting unconventional maneuvering targets. **Table 1** also illustrates that the ISMCG owns the smallest miss distance in case 1 and case 2 for complicated types of target maneuvers, and the SMCG behaves like the OSMG. In case 3 for step maneuver targets, the miss distances of ISMGC, SMCG, and OSMG are small, and there is a little difference in performance of them.

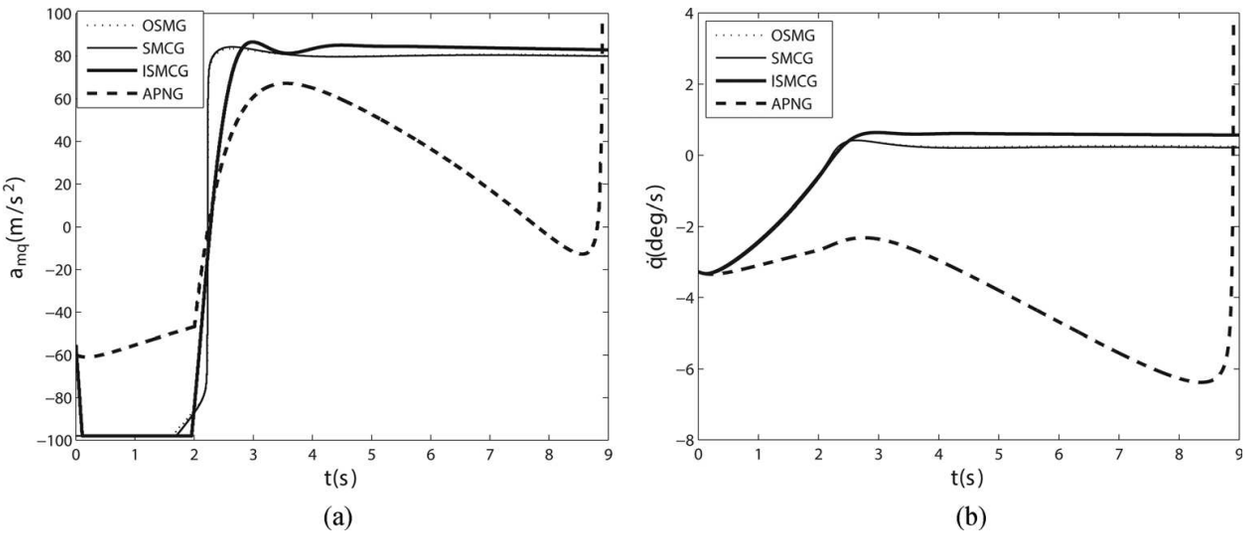


Figure 7. Guidance commands and line-of-sight angular velocities in case 3 under condition 2. (a) Guidance commands (b) Line-of-sight angular velocities.

http://dx.doi.org/10.5772/intechopen.72177

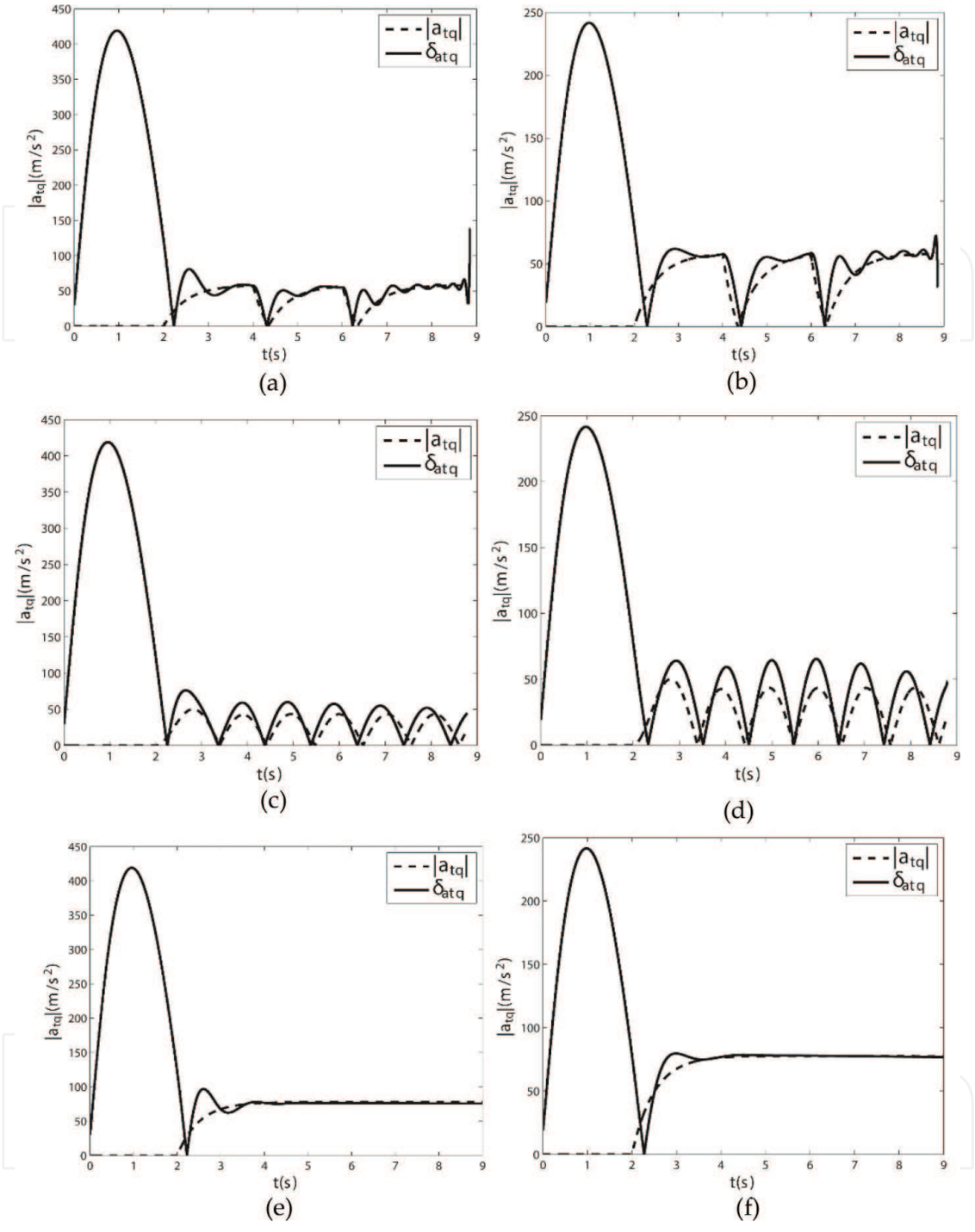


Figure 8. δ_{atq} and $|a_{tq}|$ of the ISMCG. (a) case 1 (C1); (b) case 1 (C2); (c) case 2 (C1); (d) case 2 (C2); (e) case 3 (C1); and (f) case 3 (C2).

From **Figures 2–7**, the APNG is not very appropriate to intercept complicated maneuvering targets because line-of-sight angular velocities of the APNG are greater. As a whole, the plots of the OSMG and the SMCG have little difference between each other. Their line-of-sight angular velocities are very small before the end of case 1 and case 2. Nevertheless, although continuous functions are employed to take the place of the "sgn" functions in the OSMG and the SMCG, guidance commands of the OSMCG and the SMCG all have jitters, which are

detrimental to aero fins. Line-of-sight angular velocities of the ISMCG are less than those of the APNG with the actual target's acceleration. From **Figures 2(a)**, **3(a)**, **4(a)**, and **5(a)**, in case 1 and case 2, ISMCG's guidance commands are smoother than others, which are appropriate for continuous aero surfaces to track. From **Figures 2(b)**, **3(b)**, **4(b)**, and **5(b)**, because the ISMCG uses an adaptive estimation to identify a_{tq}'s upper boundary, line-of-sight angular velocities of the ISMCG are not as moderate as those of the SMCG; however, from **Table 1**, line-of-sight angular velocities in the endgame of the ISMCG are less than those of the SMCG and the OSMG in case 1 and case 2. From **Figures 6** and **7**, the guidance commands and line-of-sight angular velocities of OSMG, SMCG, and ISMCG have little differences and are superior to those of the APNG in case 3.

From **Figure 8**, it illustrates the δ_{atq} identified by the ISMCG in three cases under two conditions. Compared with $|a_{tq}|$, in the initial 2 s, δ_{atq} is larger since $\dot{q}$ and $\widehat{k}$ are larger, and then, the tracking error decreases since the ISMCG restrains the line-of-sight angular velocity. Because δ_{atq} is not the estimation of a_{tq}, tracking phases are considered and tracking errors are not concerned. Tracking phases reflect that estimations lag behind the actual target maneuver; thereby, it decides whether the compensation $\widehat{k}$ is timely and can influence the guidance precision. With tracking phases under consideration, δ_{atq} mostly tracks $|a_{tq}|$ with a tiny time delay. In fact, for the step maneuver target in case 3, from **Figure 8(e, f)**, δ_{atq} tracks $|a_{tq}|$ well. As shown in **Table 1**, small tracking phases obtain small miss distances.

5. Conclusions

In this chapter, robust guidance schemes are presented, which require states such as initial relative speed, relative distance, and error boundaries of them besides line-of-sight angular velocity. Proposed schemes' performances are validated by simulating under uncertainties for different target's maneuver modes. Two guidance schemes hit and kill maneuverable targets with fairly limited maneuverability. By comparisons with the APNG and OSMG, the ISMCG is superior, and the OSMG and SMCG perform similarly, whereas the APNG's miss distances are greater. Moreover, guidance commands of the APNG and ISMCG are smoother than those of the OSMG and SMCG for complicated maneuver modes of the target. In conclusion, ISMCG's advantage is that the guidance scheme is not required to obtain the target acceleration under uncertain conditions for different target maneuvers.

The future work concentrates on adapting the interceptor's maximum maneuverability to be a constraint condition in the proposed guidance scheme. Anti-saturation design is studied to address the control-saturation problem in Eq. (4) [18–20].

Acknowledgements

This chapter is supported by National Key R&D Program of China under Grant Nos. 2017YFD0701000 and 2016YFD0200700, National Natural Science Foundation of China under

Grant Nos. 51475472 and 61403396, and Beijing Youth Top-notch Talent Support Program under Grant No. 2017000026833ZK23.

Author details

Jian Chen[1], Yongjun Zheng[1], Yuan Ren[2]*, Yuan Tian[3], Chen Bai[4], Zhang Ren[5], Guangqi Wang[1], Nannan Du[1] and Yu Tan[1]

*Address all correspondence to: renyuan_823@aliyun.com

1 College of Engineering, China Agricultural University, Beijing, China

2 Space Engineering University, Beijing, China

3 Beijing Institute of Space Long March Vehicle, Beijing, China

4 Beijing Institute of Aerospace System Engineering, Beijing, China

5 Beihang University, Beijing, China

References

[1] Faruqi F. Differential Game Theory with Applications to Missiles and Autonomous Systems Guidance. Hoboken: John Wiley & Sons; 2017

[2] Ben-Asher J, Speyer J. Game in Aerospace: Homing Missile Guidance. Handbook of Dynamic Game Theory. Basel: Springer; 2017

[3] Khalid S, Abrar S. A low-complexity interacting multiple model filter for maneuvering target tracking. AEU-International Journal of Electronics and Communications. 2017;**73**:157-164

[4] Jauffret C, Pérez A, Pillon D. Observability: Range-only versus bearings-only target motion analysis when the observer maneuvers smoothly. IEEE Transactions on Aerospace and Electronic Systems. 2017

[5] Zhou D, Mu C, Xu W. Adaptive sliding-mode guidance of a homing missile. Journal of Guidance, Control, and Dynamics. 1999;**22**(4):589-594

[6] Zhou D, Mu C, Ling Q. and Xu W. Optimal Sliding-mode guidance of a homing-missile. In: Kamen EW, Cassandras C, editors. 38th IEEE Conference on Decision and Control; Phoenix, USA: IEEE; 1999. pp. 5131-5136

[7] Hou Z, Su M, Wang Y. and Liu L. A fuzzy optimal sliding-mode guidance for intercepting problem. In: Camisani F, editor. IFAC World Congress; Cape Town. IFAC; 2014. pp. 3401-3406

[8] Wang Z. Adaptive smooth second-order sliding mode control method with application to missile guidance. Transactions of the Institute of Measurement and Control. 2017;**39**(6): 848-860

[9] Yang P, Fang Y, Wu Y, Yong X. Finite-time convergent terminal guidance law design based on stochastic fast smooth second-order sliding mode. Optik-International Journal for Light and Electron Optics. 2016;**127**(15):6036-6049

[10] Zhang C, Wu Y. Non-singular terminal dynamic surface control based integrated guidance and control design and simulation. ISA Transactions. 2016;**63**:112-120

[11] Song H, Zhang T. Fast robust integrated guidance and control design of interceptors. IEEE Transactions on Control Systems Technology. 2016;**24**(1):349-356

[12] Ji H, Liu X, Song Z, Zhao Y. Time-varying sliding mode guidance scheme for maneuvering target interception with impact angle constraint. Journal of the Franklin Institute. 2017

[13] Hou Z, Liu L, Wang Y, Huang J, Fan H. Terminal impact angle constraint guidance with dual sliding surfaces and model-free target acceleration estimator. IEEE Transactions on Control Systems Technology. 2017;**25**(1):85-100

[14] Zhou H, Song S, Song J. Design of sliding mode guidance law with dynamic delay and impact angle constraint. International Journal of Control, Automation and Systems. 2017;**15**(1):239-247

[15] Wheeler G, Su C, Stepanenko Y. A sliding mode controller with improved adaptation laws for the upper bounds on the norm of uncertainties. Automatica. 1998;**34**(2):1657-1661

[16] Sun L, Lian P, Chang X. Capturability of retro-augmented proportional navigation guidance law against higher speed maneuvering target. In: 21st AIAA International Space Planes and Hypersonics Technologies Conference; 6–9 March 2017. Xiamen, China: American Institute of Aeronautics and Astronautics; 2017. pp. 2203/1-2203/13

[17] Cho N, Kim Y. Optimality of augmented ideal proportional navigation for maneuvering target interception. IEEE Transactions on Aerospace and Electronic Systems. 2016;**52**(2): 948-954

[18] Turner M, Sofrony J, Herrmann G. An alternative approach to anti-windup in anticipation of actuator saturation. International Journal of Robust and Nonlinear Control. 2017;**27**(6):963-980

[19] Si Y, Song S. Adaptive reaching law based three-dimensional finite-time guidance law against maneuvering targets with input saturation. Aerospace Science and Technology. 2017;**70**:198-210

[20] Li G. and Xin M. A three-dimensional anti-saturation terminal guidance law with finite-time convergence. In: 2017 American Control Conference; 24–26 May 2017. Seattle, USA: IEEE; 2017. pp. 2243-2248